MICROSTRUCTURAL RESPONSE OF Ti6Al4V ELI ALLOYED WITH MOLYBDENUM BY DIRECT ENERGY DEPOSITION

N.K.K. Arthur[1, 2], C. Siyasiya[2], S. Pityana[1], M. Tlotleng[1]

[1]CSIR, NLC, Laser Enabled Manufacturing Group, Pretoria Campus, 0001, South Africa

[2]University of Pretoria, Dept. of Materials Science and Metallurgical Engineering, Pretoria, 0001, South Africa

*NArthur@csir.co.za, charles.siyasiya@up.ac.za, SPityana@csir.co.za, MTlotleng@csir.co.za

Keywords: In Situ Alloying; Directed Energy Deposition; Ti6Al4V; Beta Stabilizers; Fish Scaling; Solidification Structure; Omega Phase

Abstract

Alloy development opens the way to create new materials for specialized processes, and attain materials that are usually difficult to acquire. Property enhancements and part performance is achievable in an exciting new way when this technique of producing materials is coupled with additive manufacturing technologies. This study explores the use of direct energy deposition technique of additive manufacturing processing for alloy development. The aim was to improve the ductility and subsequent part performance of LENS produced titanium alloys. In this study, the investigated heat inputs proved effective in producing homogenous molybdenum added Ti6Al4V microstructures. Consequently, the addition of the β-stabilizing alloying element, molybdenum, did not only result in the increased volume fraction of the β-phase but also the change from planar to cellular solidification. Thus, the hardness values for molybdenum additions of 10 mass percentage were found to be in the range of 200±34 $HV_{0.3}$, and this was attributed to the β-stabilizing and grain refining effect of refractory metals such as molybdenum.

1. Introduction

Despite the many benefits inherent to the additive manufacturing (AM) processes, coupled with the achievable properties of several alloys presently in use, some limitations prevent the applicability and adoption of AM for more than rapid prototyping applications. One such limitation is in the fatigue life of titanium alloy 3D printed parts as reports indicate that these parts typically fail sooner in contrast to conventionally produced parts [1]. The fatigue life of a material refers to the number of cycles at a particular stress level, which results in failure in the part [2] [3]. Another cause of reduced part performance or failure is the high residual stress (RS) build up in the material due to high thermal gradients experienced during fabrication [4].

This RS build-up would result in a significant increase in material strength while reducing ductility of the 3D printed material [4]. This ultimately reduces the effective life of AM parts in service.

Directed energy deposition (DED) technique performed on the laser engineered net shaping (LENS) system is a specialized technique that produces high-density parts from a wide range of alloy materials. Furthermore, refurbishment applications are possible with this system due to its flexibility and capability to produce parts with more than one material at a time. This capability is specifically useful in development of functionally graded materials (FGMs) and alloy development processes. This was the technique used in this work to 3D print Ti6Al4V ELI alloy samples.

Alloying is a beneficial method for enhancing the properties of materials, particularly in response to a need arising from in-service challenges experienced. This leads to the development of a novel material that exhibits improved performance linked to the microstructure of the new material. The evolved microstructure is dependent on the processing conditions and compositions of alloying elements [5]. Vrancken et al. [6] considered the alloying of titanium alloys with Molybdenum (Mo) to explore the capability of selective laser melting (SLM) for creating new materials. This study found that the Mo addition improved the properties of the titanium alloy in comparison to conventional β-alloys. Fischer et al. [7] considered the combination of Ti-Nb produced by SLM for medical applications due to the achievable strength and biocompatibility of the materials. The outcomes stated that mixing of powders for alloying with AM was an effective method as it opened up opportunities to produce difficult to acquire materials.

Xie et al. [8] demonstrated how various energy influences could result in material property improvements of titanium alloys. The authors investigated electro-shocking treatment

(EST) with the aim of optimizing the microstructure and comprehensive mechanical properties of titanium alloys. This technique introduced thermal conditions that led to a phase transformation from α to β, and reported an increase in β-phase fraction of approximately 6% after application of EST for 0.04 s. It is worth noting that the application of EST resulted in a phase transformation accompanied by an improvement in texture intensity, and a change in the α-phase texture direction from the X_0 to the Y_0 direction, and the β-phase from the Y_0 to the X_0 texture direction. The results observed by investigators showed that EST was an effective technique to optimize the microstructure of the TC11 alloy investigated.

This study explores the use of alloying elements for material property improvements, and discusses two approaches of alloying Ti6Al4V alloy with Mo via DED processing to improve the ductility of the Ti6Al4V alloy. Parts produced by DED on the LENS system are characterized by high strength and poor ductility, with tensile elongation less than 10%. Available literature on similar work that was focused on SLM processing identified Mo additions of about 10 mass % as suitable to stabilize the β-phase and attain an improvement in ductility. This study assesses the two processing conditions or alloying approaches to establish feasibility, and which yields greater results towards improving ductility of Ti6Al4V parts produced by LENS. The discussion highlights the attained results vis-à-vis the processing conditions, alloy additions and resultant microstructure.

2. Materials and Methods

2.1. Material Characterization

Mixing of Grade 23 Ti6Al4V ELI alloy (Ti-64) with elemental Mo metal powder produced the feedstock material used in this study. Mixing of powders in a tubular mixer for 30 minutes at varying Mo content gave powders with expected compositions of 10, 15 and 20 mass

percentage (mass %). Powder characterization took place by means of a JEOL JSM-6510 scanning electron microscope-energy dispersive spectroscopy (SEM-EDS) for morphology and chemical composition confirmation.

Ti-64 characterization took place by way of standardized powder measurement methods for AM powders as specified in ASTM F3049-14. The nitrogen and oxygen contents in the powder were analyzed using an ELTRA OHN 2000 inert gas combustion analyzer, while the elemental composition analysis was performed using an ARCOS Spectro ICP-OES instrument. The Microtrac SI/S3500 instrument used aided in particle size distribution (PSD) determination of the powders. The results and discussions following refer to Grade 23 Ti6Al4V ELI alloy, however, the abbreviation Ti-64 is used, and the "ELI" suffix dropped.

The use of x-ray diffraction (XRD) and electron backscatter diffraction (EBSD) in conjunction with microscopy techniques aid in the characterisation of the microstructures and reveal the presence of specific phases and their differences. The EBSD technique employs a Zeiss Cross Beam 540 FIB-SEM with Oxford Atlas software for pattern acquisition and analysis of grain size maps to reveal information about the crystal structure and orientation, phase(s) present and material strain. The equipment employed for XRD analysis is a PANalytical Empyrean system that has a Cu k alpha x-ray tube. Pattern measurement typically occurs at a voltage of 45 kV and a beam current of 40 mA, with PANalytical High Score Plus software with Rietveld refinement linked to the latest International Centre for Diffraction Data (ICDD) reference patterns.

2.2. Laser Deposition

The processing of materials was performed by way of the DED technique on the LENS™ 850-R system mounted with a 1 kW IPG fiber laser and a co-axial powder delivery nozzle. The powder is stored in a storage system known as a hopper and fed through the system and out of

the nozzles for fabrication. The dual hopper system enables the feeding of multiple materials at a go to blend the materials mid-processing to perform in situ alloying operations.

The powder flow rates at the employed rpm setting values of the system were determined by timing the amount of powder delivered (in grams) in a plastic container over a 1-minute interval. Grade 5 Ti6Al4V alloy plates of 6.5 mm thickness were prepared by sandblasting to increase surface roughness and prevent laser reflection during processing, and cleaned with acetone to remove any oils and impurities from the surface of the plate. Laser deposition took place in a controlled atmosphere process chamber to maintain an inert atmosphere with oxygen content below 10 ppm (to reduce oxidation of part being manufactured [9]).

Test coupons of 12 x 12 x 5 mm dimensions were laser printed to produce three sets of samples for evaluation. The first set consisted only of Ti-64 powder coupons as control (designated 'as-built' for ease of identification). The second set consisted of the pre-mixed Ti-64 + xMo powder compositions (where x is 10, 15 or 20 mass %). For the third set of samples, a dual powder feeding system allowed the introduction of powders simultaneously into the melt pool for deposition to proceed via in situ processes (LENS blend). Adjusting powder flow rates for the third set ultimately resulted in a change in material composition that resulted in the samples with 10, 15 or 20 mass %.

An energy density (ED) range of 200 – 300 J/mm^3 provided sufficient heat input necessary to produce coupons with minimal porosity levels (in the Ti-64 samples) for evaluation [10] [11]. The ED is an expression that relates the laser power, scan speed, layer thickness and hatch spacing together in an equation that defines the relationship between these parameters. This equation, as expressed in Attar et al. [12] and Tang, et al. [13], is:

$$E = \frac{P}{v\,x\,h\,x\,t} \qquad \text{Eq. 1}$$

Where P is the laser power (W), v is the laser scanning speed (mm/s), h is the hatch spacing (mm) and t is the layer thickness (mm).

The Ti-64 powder mixed with elemental Mo to produce sample coupons was termed “pre-mixed” while the sample coupons produced by feeding material simultaneously through two separate feeding systems and directly into the melt pool was termed “LENS blend”. This study compares and discusses the results thereof.

2.3. Metallurgical Sample Preparation

A conductive resin was used to mount each sample that was cross-sectioned for metallography analyses. Samples were ground using SiC grinding papers with water as a lubricant. The process made use of four different SiC grit-size grinding papers, namely 80, 320, 1200 and 4000 grit size. A polishing stage after grinding produced the desired mirror-finish surface by means of an Md-Chem cloth with a 0.04 μm suspension. Treatment of the mirror-finish surface with Kroll’s reagent revealed the microstructure for observation.

An Olympus BX51M microscope together with Stream Essentials software aided in microstructural observations, while hardness profile investigations carried out was through a Matsuzawa Vickers micro-hardness tester. The load applied was 300 grams at a dwelling time of 10 seconds, while employing a spacing of 250 μm between the indentations. Approximately 15 to 30 indentations proved sufficient to cover the various regions of the samples.

3. Results and Discussions

3.1. Material Characterization

The various materials used for laser deposition were prepared and characterized to confirm its suitability for laser processing. The different powder samples employed included one sample

made of Ti-64 without Mo additions (as-built), while the remaining three powder samples comprised of a mixture of Ti-64 powder with systematically varied elemental Mo powder content.

Table 1 presents a comparison of Ti6Al4V alloy grades and its allowable limits of each element based on the grade. The observation made is that the Ti-64 feedstock material used for deposition compares well with the requirements set out in ASTM F136.

Figure 1 presents a SEM image of the pre-mixed powder with varying Mo content. The objective was to attain a homogeneous mixture for use in laser deposition. Observations made from SEM-EDS analysis reported lower Mo content than the intended mixed amounts. The difference in Mo content reported by SEM-EDS from actual mixed amount showed a decrease in the range of 20 to 30 mass %, which implies that homogeneity was possibly not achieved and would likely lead to sample coupons that showed inhomogeneous microstructures. The implication is that this inconsistency could potentially compromise process repeatability, and limit the achievement of a homogenous microstructure. This is consistent with observations and concerns stated by Chlebus et al. [14], Fischer et al. [7], and Kinnear et al. [15]. Further material deficiencies observed include internal defects sighted on the Ti-64 powder particles, Figure 1 (a), which are potential sources of porosity in the deposited material if not closely monitored to mitigate their effects.

3.2. Microstructure and Hardness Properties

Process development is essential for identification of a suitable parameter set for laser deposition when considering alloy development. Since Ti6Al4V (1660°C) and Mo (2623°C) possess differing melting points, placing emphasis on the thermodynamics of the system is of importance. Selection of suitable processing parameters were determined based on thin wall

and cube depositions (Figure 2 (a) and Figure 2 (b) respectively) that reported dimensional accuracy and minimal porosity respectively as illustrated in Figure 3 (a) and Figure 3 (b).

Refractory materials are highly resistant to heat and wear [16] therefore, higher energy inputs are necessary for sufficient melting of the added Mo to ensure its dissolution into the matrix. Thus, testing of two ED inputs (235 & 287 J/mm^3) allowed a comparative analysis to evaluate the efficiency of the process variables, and extent of Mo dissolution due to the DED processing.

Figure 3 illustrates the influence of the ED on the microstructural evolution of Ti-64 parts produced by DED technique performed on the LENS to produce the as-built samples. As may be seen, it was observed that the higher ED of 287 J/mm^3, Figure 3 (b), resulted in a smoother and more homogenous microstructure which was free of what is termed the "fish-scale" effect (Figure 3 (a)). The so-called fish-scale effect occurs when the melt pool shape changes and resembles overlapping weld beads [17]. Its occurrence is evident at lower powers when the energy input (e.g. 235 J/mm^3) does not adequately melt the material to give a homogenous microstructure. This phenomenon causes grains to grow radially towards the center of each melt pool with the consequence of a random grain orientation and texture [17]. The less prominent microstructural evolution observed in Figure 3 (c) as compared to Figure 3 (d) (whereby prior columnar β grains are more pronounced) illustrates the effect of fish scaling and the effect of inadequate process parameters on microstructural evolution.

A higher laser power is therefore preferred as it promotes a strong texture, parallel melt pool boundaries that are flat and wide, in addition to columnar grains (Figure 3 (d)) that grow vertically [17] [18]. Therefore, the deduction is that the ED of 287 J/mm^3 is better suited for Mo processing for alloy development. The energy density used to produce Ti-64 samples with the lowest extent of porosity was the parameter set selected for alloy development investigations [11] [10]. The selection of two ED values for processing allowed for comparison

of the effects of a lower and higher heat input on Ti-64 material prior to and after treatment with Mo additions.

The fine (α+β) mixed microstructure observed in Figure 3 is characteristic of AM produced Ti6Al4V alloys. A number of different microstructural phases were achievable depending on the cooling rate and composition. As can be seen from Figure 3 (e), the clear difference in microstructure could be attributed to the presence of acicular α' martensite that developed upon DED fabrication of the Ti-64 after being cooled to below the β-transus temperature at higher cooling rates of above 18 $°Cs^{-1}$ [19]. The Widmanstätten (α+β) mixture observed in Figure 3 (f) evolved due to lower cooling rates of approximately 2 $°Cs^{-1}$ [19], which resulted from the in situ decomposition of the α' martensite. The process occurs via a diffusion-controlled nucleation that leads to the growth of stable α and β phases [20]. This gives rise to α+β lamellar structures appearing in colonies. These colonies are characterized by the α-phase lamellae found within a β-phase matrix [19]. This Widmanstätten microstructure is reported to exhibit elevated yield and tensile strength in addition to improved tensile elongation [21]. This is contrary to what is observed from tensile investigations of LENS produced AM specimen [10] [22], driving the necessity for the optimization of the alloy development and AM production process in pursuit of the improved material integrity and part performance.

Recently, Beyl [22] studied the tensile properties of Ti-64 alloy specimen produced with LENS AM, investment casting (IC) and wrought processes. The lamellar microstructure of conventional IC and wrought processes reported lower yield and tensile strengths compared to the LENS specimen, however, the LENS specimen showed the lowest tensile elongation (below 10%). The observation of reduced tensile elongation reported by Beyl [22] compares well with observations by Arthur & Pityana [10].

Figure 4 illustrates the effect of the addition of Mo on the evolution of the microstructures of the DED produced Ti-64 samples. As may be seen, it would appear the

volume fraction of the undissolved Mo particles increased with the Mo content (Figure 4 (a) to (c) and (d) to (f)). As expected, the Mo particles dissolved more with an increase in the energy density i.e. from 235 to 287 J/mm^3. Similar observations identified by various authors when investigating in situ alloying of Ti6Al4V with refractory metals by powder bed fusion (PBF) compares well with the current observations [14] [7] [6]. These investigators reported the presence of undissolved refractory particles.

Moreover, the undissolved particles (alloying elements) show some degree of segregation towards the edges and lower ends of the build samples. This compares well with literature reported by Appel and Oehring [5]. Investigations conducted by Griffiths et al. [23], as well as Vrancken et al. [6] reported some segregation of alloying elements and was attributed to the partitioning of these elements during the solidification process, Figure 4 (c) and (f). This would mostly likely cause an uneven distribution of the dissolved Mo in the matrix and consequently affect mechanical properties negatively. It is worth stating that the pre-mixing approach identified from literature is the common approach employed by investigators when performing in situ alloying. Studies performed by Madikizela at al. [24] compared the mechanical properties of a commercial β-alloy with that of a β-alloy processed by in situ alloying on a SLM system. The commercial alloy reported superior properties to the in situ alloy, which led investigators to the conclusion that in situ alloying was not a viable solution due to the microstructural inhomogeneity observed.

Figure 5 compares the evolution of the microstructures of the approach utilizing the pre-mixed alloy versus those of the approach utilizing the LENS blend alloys. Both alloys contained 20 mass % Mo and were produced at a heat input of 287 J/mm^3. The SEM-EDS analysis confirmed an increased amount of Mo at lower regions (Figure 5 (e) & (f)) as compared to the mid (Figure 5 (c) & (d)) and top (Figure 5 (a) & (b)) sections. An average Mo content of 19.81 mass % was reported for the pre-mixed materials and 21.09 mass % for the

LENS blend materials, respectively. Contrary to the concerns from powder analysis of the pre-mixed material that reported Mo composition between 13 to 17% instead of 20%, the reported composition after fabrication infers a significant amount of Mo dissolved into the matrix.

In spite of the similarities that existed in the microstructures evolved from both samples, it is important to note that the bottom section of the pre-mixed sample shows presence of columnar prior β-grains, while the middle and top sections show some fish scale effect. The presence of columnar grains in the pre-mixed β-alloy suggests planar solidification, as experienced in Ti6Al4V alloys. Fish scale effect occurs when the laser power or energy input required for material processing is low. Therefore, the deduction made is that the heat input for the pre-mixed process condition was low, in contrast to observations made for the LENS blend process condition. Although present to a small extent, overcoming the effect of fish scaling was possible through the LENS blend process condition with material fed simultaneously into the melt pool for alloying.

As the Mo content increased, the solidification mechanism shifted from planar to cellular solidification. In other words, the extent to which this occurred was dependent on the composition. As expected, segregation of the alloying elements accompanies the shift to cellular solidification. Furthermore, the addition of the Mo does not only change the solidification mechanism, but reduction of grain size, Figure 5. In other words, thinner and smaller β-grains begin to form within the melt pool, along with what resembles dendrites. This observation compares well with literature, which states that the evolving solid/liquid interface morphology can be planar, cellular or dendritic based on the material composition or solidification conditions as influenced by process variables [25].

Figure 6 illustrates the effect of the addition of Mo on the phase fraction of the processed alloys, based on process conditions, while Table 2 and Table 3 indicate the phase fractions associated with these alloys. Figure 6 (a) and (b) represent the as-built alloys

processed at 235 and 287 J/mm^3 respectively, with the dominant hexagonal close packed (hcp) α-Ti accounting for over 90% (Table 2) of the phase fraction in both alloys (represented by the red color). Upon analysis of the 10% Mo pre-mixed and LENS blend alloys, processed at 287 J/mm^3, a noticeable increase in β-Ti (Table 3) was observed (Figure 6 (d)), whereas the pre-mixed alloy (Figure 6 (c)) showed no significant difference. The inconsistency of mixing associated with the pre-mixing process is the reason attributed to this. However, the 20% Mo additions of the pre-mixed and LENS blend alloys (Figure 6 (e) and (f)) both reported an increase in β-phase, with β-Ti reported as the dominant phase in each case. Furthermore, alloys that showed an increase in β-Ti fraction reported a decrease in hardness as anticipated. The reason for this is that the crystal structure of β-Ti is softer than that of α-Ti, owing to an increased amount of slip planes at different orientations [3].

Figure 7 represents the XRD patterns of the pre-mixed and LENS blend alloys with 20% Mo additions that were 3D printed at an ED of 287 J/mm^3. A comparison of XRD and EBSD analyses reveals similar phases identified by the two techniques, that is to say α (hcp) and β (bcc); however, it reports these phases in different amounts. In addition, the lattice parameters associated with the identified phases are 2.94 Å (a) and 4.68 Å (c) for the α-phase, and 3.327 Å (a) for the β-phase. While EBSD analysis allows for targeted analysis of sample surfaces, XRD analysis reveals a broader scope relating to the bulk material. This accounts for the difference in phase amounts reported for the two techniques. Moreover, the fitting suggests that there is another hexagonal phase identified, particularly in the alloys with Mo additions, and reports lattice parameters of 4.60 Å (a) and 2.82 Å (c).

Literature reports the presence of hexagonal omega (ω) as a non-equilibrium phase that develops when alloying titanium and its alloys with transition metals like Mo [26]. This metastable phase typically forms upon quenching from a temperature above the β-transus, and is identifiable as small densely distributed particles [27]. Gragg [28] reported the lattice

parameters of ω-phase as 4.60 Å (a) and 2.82 Å (c), which corresponds to XRD results of the present study, and confirms the presence of ω-phase in the pre-mixed and LENS blend alloys represented by Figure 7.

The alloys with Mo additions reveal a similar pattern to that of the Ti-64 alloys; however, it is worth noting that the peak intensity of the alloys with Mo additions generally increased as the Mo content increased, while the 20% Mo pre-mixed alloy reported higher intensity than the LENS blend allow (Figure 7). This implies a reliance of the grain orientation on the Mo content.

Figure 8 shows the variation of hardness with an increase in the Mo content of the alloy. As may be seen, the hardness response of the alloys correlated with the microstructures as the Mo content was increased. This observation corroborates EBSD phase analysis results. The faster cooling in as-built alloys produced at an ED of 235 J/mm^3 results in α' martensite structure (Figure 3 (e)) which resulted in elevated hardness values (405±15 $HV_{0.3}$). The Widmanstätten (α+β) mixture (Figure 3 (f)) was as a result of the in situ decomposition of α' martensite of the as-built alloys produced at an ED of 287 J/mm^3. The cooling rates thereof being significantly lower than that required to form α' martensite, thus it is anticipated that a softening effect in comparison to α' martensite would result in lower hardness values (380±13 $HV_{0.3}$).

Pre-mixed alloys generally produced lower hardness values than as-built alloys, while pre-mixed produced at 235 J/mm^3 reported lower hardness values than that at 287 J/mm^3. Conversely, the LENS blend process condition of 10% and 15% Mo content alloys reported lower hardness values at 287 J/mm^3 (206±34, 200±24 $HV_{0.3}$ respectively) than the pre-mixed process condition of similar alloys produced at both ED (235 and 287 J/mm^3). This was attributed to an increased amount of β-phase present (Figure 6 (d)) that promotes a softening of the material, which is also associated with an increase in ductility. Hardness values reported

for the LENS blend of 20% Mo content alloy showed an increase (324±13 $HV_{0.3}$) as compared to that of 10% and 15% Mo content, however, the reported hardness values were lower than its as-built and pre-mixed alloy counterparts were.

The LENS blend alloys reported lower hardness values at a 10% and 15% Mo content compared to the commercial β alloy (Ti-3Al-8V-6Cr-4Zr-4Mo) investigated by Madikizela et al. [24], which reported a hardness value of 309±9 $HV_{0.3}$. Furthermore, the SLM processed in situ alloy of Ti6Al4V+10%Mo investigated by Vrancken et al. [6] reported a hardness value of 338±6 $HV_{0.3}$, which saw a slight decrease to 336±4 $HV_{0.3}$ upon heat treatment at 1050 °C to reveal a fully β microstructure. This change, however, is negligible. This result was comparable to the LENS blend alloy of 20% Mo content of this work. This suggested that the DED process has potential to produce alloys with comparable microstructures and mechanical properties as commercial and heat-treated alloys.

4. Conclusions

An investigation that compared the pre-mixed and LENS blend alloy DED processes took place, and led to the following conclusions:

- The simultaneous feeding approach of the LENS blend is consequently more practical than the pre-mixing approach, as production of various samples at different compositions are easily attainable in a shorter time and at lower cost.
- The LENS blend approach resulted in a more efficient process as it achieved optimal microstructures and hardness properties. The significantly decreased hardness values reported for the LENS blend alloys of Ti-64 with Mo additions in comparison to the Ti-64 as-built alloys demonstrated this. This implies a reduced β-transus temperature and the stabilization of the β-phase.

- The control the LENS blend process offers addressed concerns about the homogeneity of mixing and the repeatability in process.
- The response of the alloys to thermal cycles experienced through LENS DED processing indicated that a homogenous microstructure is achievable at an ED of 287 J/mm^3 and greater (with reduced porosity and no visible fish scale defects), and is better suited for processing of Ti6Al4V ELI alloyed with 5 to 20 mass% Mo additions.

References

[1] B. McManus, "www.brilliant.org/realengineering," Real Engineering, [Online]. Available: https://www.youtube.com/watch?v=fzBRYsiyxjI&list=WL&index=13&t=0s. [Accessed 21 April 2020].

[2] W. D. Callister and D. G. Rethwisch, Materials Science and Engineering: An Introduction, Hoboken, New Jersey: John Wiley & Sons, Inc., 2014.

[3] G. E. Dieter, Mechanical Metallurgy, London, England: McGraw-Hill Book Company, 1988.

[4] J. J. Lewandowski and M. Seifi, "Metal Additive Manufacturing: A Review of Mechanical Properties," *Annual Review of Materials Research,* vol. 46, pp. 151 - 186, 2016.

[5] F. Appel and M. Oehring, "Gamma-Titanium Aluminide Alloys: Alloy Design and Properties," in *Titanium and Titanium Alloys: Fundamentals and Applications*, Weinheim, Germany, WILEY-VCH Verlag GmbH & Co. KGaA, 2003, pp. 89 - 152.

[6] B. Vrancken, L. Thijs, J. P. Kruth and J. Van Humbeeck, "Microstructure and Mechanical Properties of a Novel Beta Titanium Metallic Composite by Selective Laser Melting," *Acta Materialia,* vol. 68, pp. 150-158, 2014.

[7] M. Fischer, D. Joguet, G. Robin, L. Peltier and P. Lahuerte, "In situ Elaboration of a Binary Ti–26Nb Alloy by Selective Laser Melting of Elemental Titanium and Niobium Mixed Powders," *Materials Science and Engineering,* vol. 62, no. C, pp. 852 - 859, 2016.

[8] L. Xie, C. Liu, Y. Song, H. Guo, Z. Wang, L. Hua, L. Wang and L.-C. Zhang, "Evaluation of Microstructure Variation of TC11 Alloy after electroshocking Treatment," *Journal of Materials Research and Technology,* vol. 9, no. 2, pp. 2455-2466, 2020.

[9] A. Bandyopadhyay, B. V. Krishna, W. Xue and S. Bose, "Application of Laser Engineered Net Shaping (LENS) to manufacture porous and functionally graded structures for load bearing implants," *Journal of Materials Science: Materials in Medicine,* vol. 20, pp. 29 - 34, 2009.

[10] N. K. K. Arthur and S. Pityana, "Microstructure and Material Properties of LENS Fabricated Ti6Al4V Components," *R&D Journal of the South African Institution of Mechanical Engineering,* vol. 34, pp. 33 - 36, 2018.

[11] N. K. K. Arthur, "Laser Based Manufacturing of Ti6Al4V: A Comparison of LENS and Selective Laser Melting," *Materials Science Forum,* vol. 950, pp. 44 - 49, 2019.

[12] H. Attar, M. Bonisch, M. Calin, L. C. Zhang, S. Scudino and J. Eckert, "Selective Laser Melting of In Situ Titanium-Titanium Boride Composites: Processing, Microstructure and Mechanical Properties," *Acta Materialia,* vol. 76, pp. 13 - 22, 2014.

[13] M. Tang, C. P. Pistorius and J. L. Beuth, "Prediction of Lack-of-Fusion Porosity for Powder Bed Fusion," *Additive Manufacturing,* vol. 14, pp. 39-48, 2017.

[14] E. Chlebus, B. Kuznicka, R. Dziedzic and T. Kurzynowski, "Titanium Alloyed With Rhenium by Selective Laser Melting," *Materials Science & Engineering,* vol. 620, no. A, pp. 155 - 163, 2015.

[15] A. Kinnear, T. C. Dzogbewu, I. Yadroitsava and I. Yadroitsev, "In-Situ Alloying Process of Ti6Al4V-xCu Structures By Direct Metal Laser Sintering," in *Proceedings of the 17th International Conference for Rapid Product Development Association of South Africa*, Vanderbijl Park, Vaal, South Africa, 2016.

[16] D. Olsen, "Metal Tek International," 24 November 2020. [Online]. Available: https://www.metaltek.com/blog/refractory-metals/. [Accessed 27 January 2021].

[17] H. Choo, K.-L. Sham, J. Bohling, A. Ngo, X. Xiao, Y. Ren, P. J. Depond, M. J. Matthews and E. Garlea, "Effect of Laser Power on Defect, Texture, and Microstructure of a Laser Powder Bed Fusion Processed 316L Stainless Steel," *Materials and Design,* vol. 164, 2019.

[18] B. Jared, "Defect Detection in Metal Additive Manufacturing Through Apllication of In-Situ Diagnostics," 2019. [Online]. Available: https://www.osti.gov/servlets/purl/1641629. [Accessed 16 December 2020].

[19] J. Sieniawski, W. Ziaja, K. Kubiak and M. Motyka, "Microstructure and Mechanical Properties of High Strength and Two-Phase Titanium Alloys," in *Titanium Alloys - Advances in Properties Control*, Weinheim, Germany, WILEY-VCH Verlag GmbH & Co. KGaA, 2013.

[20] Y. Han, W. Lu, T. Jarvis, J. Shurvinton and X. Wu, "Investigation on the Microstructure of Direct Laser Additive Manufactured Ti6Al4V Alloy," *Materials Research,* vol. 18, no. Suppl. 1, pp. 24 - 28, 2015.

[21] W. Xu, M. Brandt, S. Sun, J. Elambasseril, Q. Liu, K. Latham, K. Xia and M. Qian, "Additive Manufacturing of Strong and Ductile Ti–6Al–4V by Selective Laser Melting Via In Situ Martensite Decomposition," *Acta Materialia,* vol. 85, pp. 74 - 84, 2015.

[22] K. Beyl, *Investigation Into Microstructural and Mechanical Properties of a Ti6Al4V Hybrid Manufactured Component,* MEng Dissertation. North West University. Available at: http://repository.nwu.ac.za/handle/10394/36192 (Accessed: 20 January 2021), 2020.

[23] M. L. Griffith, M. T. Ensz, J. D. Puskar, C. V. Robino, J. A. Brooks, J. A. Philliber, J. E. Smugeresky and W. H. Hofmeister, "Understanding the Microstructure and Properties of Components Fabricated by Laser Engineered Net Shaping," 2000. [Online]. Available: https://www.cambridge.org/core/journals/mrs-online-proceedings-library-archive. [Accessed 13 December 2020].

[24] C. Madikizela, L. A. Cornish, L. H. Chown and H. Moller, "Microstructure and Mechanical Properties of Selective Laser Melted Ti-3Al-8V-6Cr-4Zr-4Mo Compared to Ti-6Al-4V," *Materials Science and Engineering A,* vol. 747, pp. 225 - 231, 2019.

[25] F. Yan, W. Xiong and E. J. Faierson, "Grain Structure Control of Additively Manufactured Metallic Materials," *Materials,* vol. 10, p. 1260, 2017.

[26] M. Sabeena, S. Murugesan, R. Mythili, A. K. Sinha, M. N. Singh, M. Vijayalakshmi and S. K. Deb, "Studies on Omega Phase Formation in Ti-Mo Alloys Using Synchrotron XRD," *Transactions of the Indian Institute of Metals,* vol. 68, no. 1, pp. 1-6, 2015.

[27] P. Zhanal, P. Harcuba, J. Strasky, J. Smilauerova, P. Beran, T. C. Hansen, H. Seiner and M. Janecek, "Transformation Pathway Upon Heating of Metastable Beta Titanium Alloy Ti-15Mo Investigated by Neutron Diffraction," *Materials,* vol. 12, no. 21, 2019.

[28] J. E. Gragg, "The Omega Phase in Titanium-Vanadium Alloys," Rice University, Houston, Texas, 1964.

Table 1: Comparison of Ti6Al4V alloy chemical compositions allowable limits

Material	Element, mass %							
	N	C	H	Fe	O	Al	V	Ti
Ti6Al4V ELI (feedstock material)	0.0093	0.006	0.001	0.25	0.056	5.95	4.03	89.70
Gr. 5 Ti6Al4V (ASTM F1472)	0.05 (max)	0.08 (max)	0.015 (max)	0.3 (max)	0.2 (max)	5.5 – 6.75	3.5 – 4.5	88.11 (balance)
Ti6Al4V ELI (ASTM F136)	0.05 (max)	0.08 (max)	0.012 (max)	0.25 (max)	0.13 (max)	5.5 – 6.5	3.5 – 4.5	88.48 (balance)

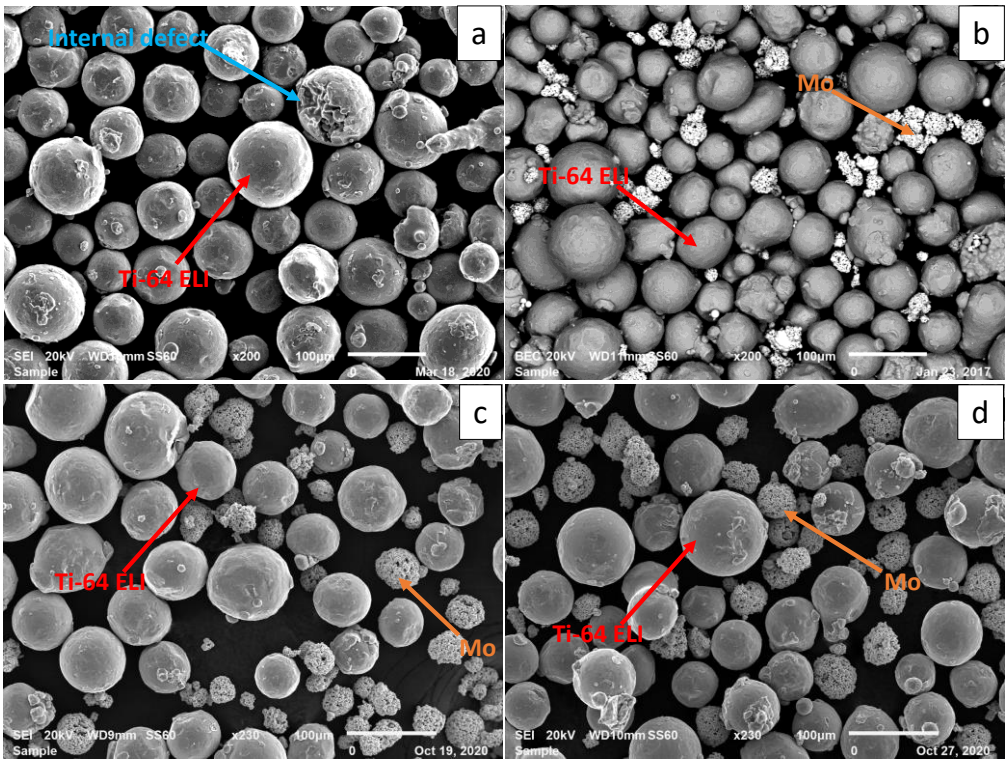

Figure 1: Ti6Al4V ELI powder pre-mixed with elemental molybdenum (a) Ti-64 + 0% Mo, (b) Ti-64 + 10% Mo, (c) Ti-64 + 15% Mo, and (d) Ti-64 + 20% Mo

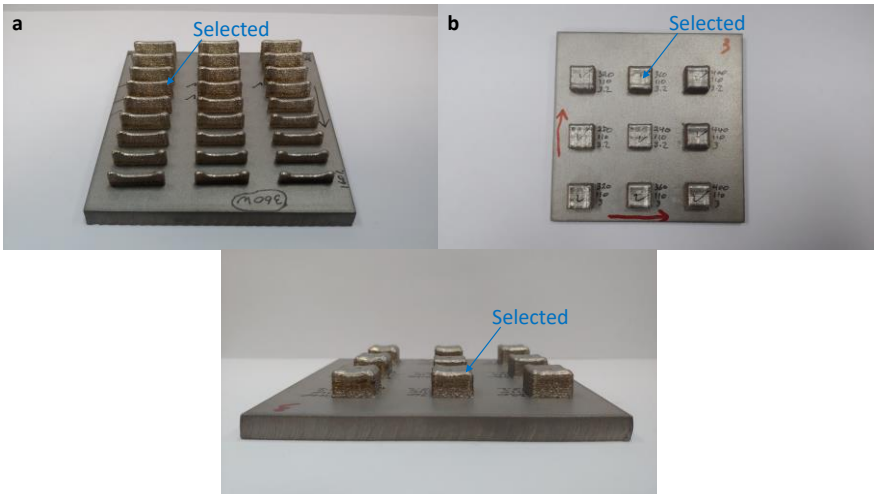

Figure 2: Sample coupons produced for investigations, (a) thin wall and (b) cube

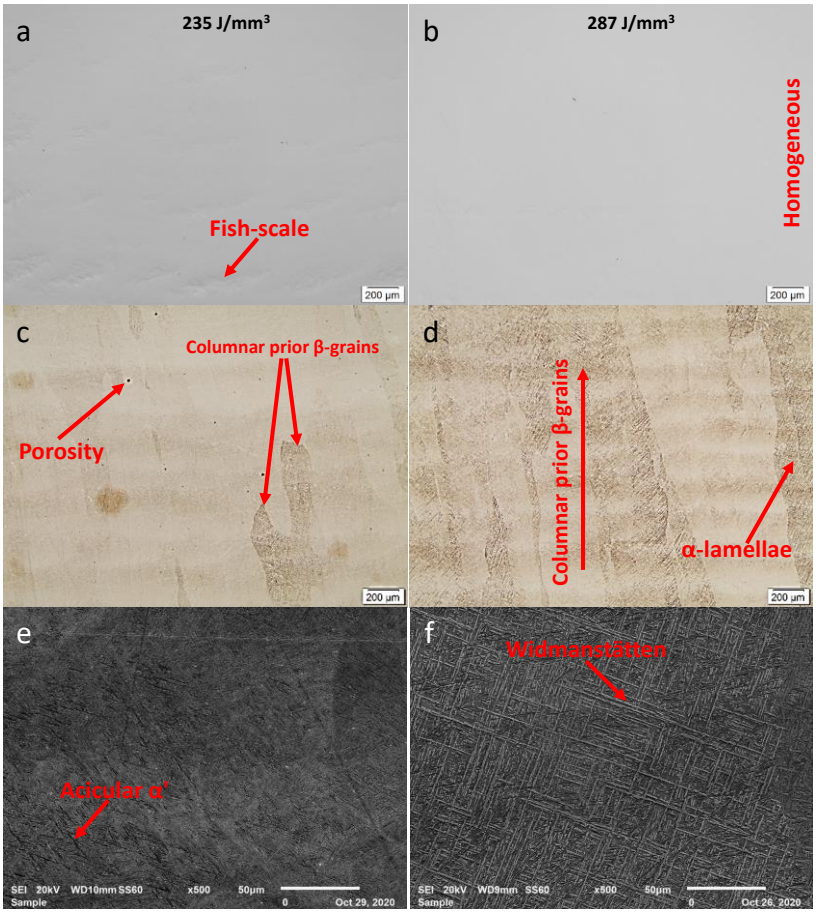

Figure 3: Influence of energy density on microstructure of Ti6Al4V ELI. Optical micrographs pre-etching (a, b), Optical micrographs post-etching (c, d), SEM micrographs (e, f).

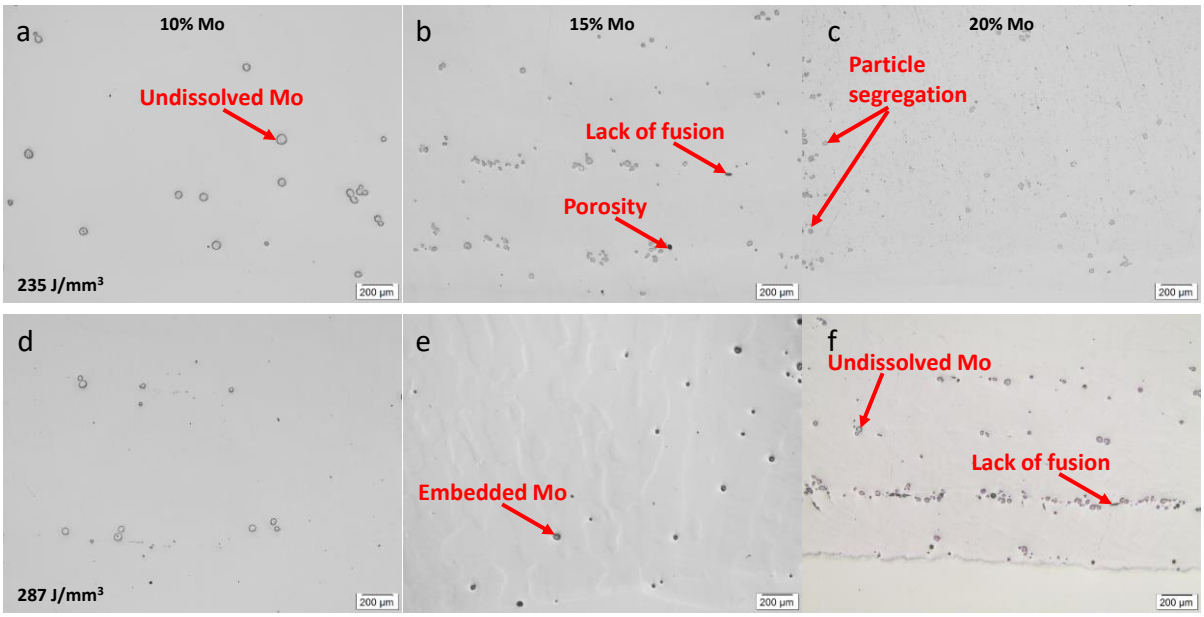

Figure 4: Optical images of pre-mixed Ti6Al4V ELI with increasing amounts of Mo additions (left to right) deposited at low to high energy densities (top to bottom respectively).

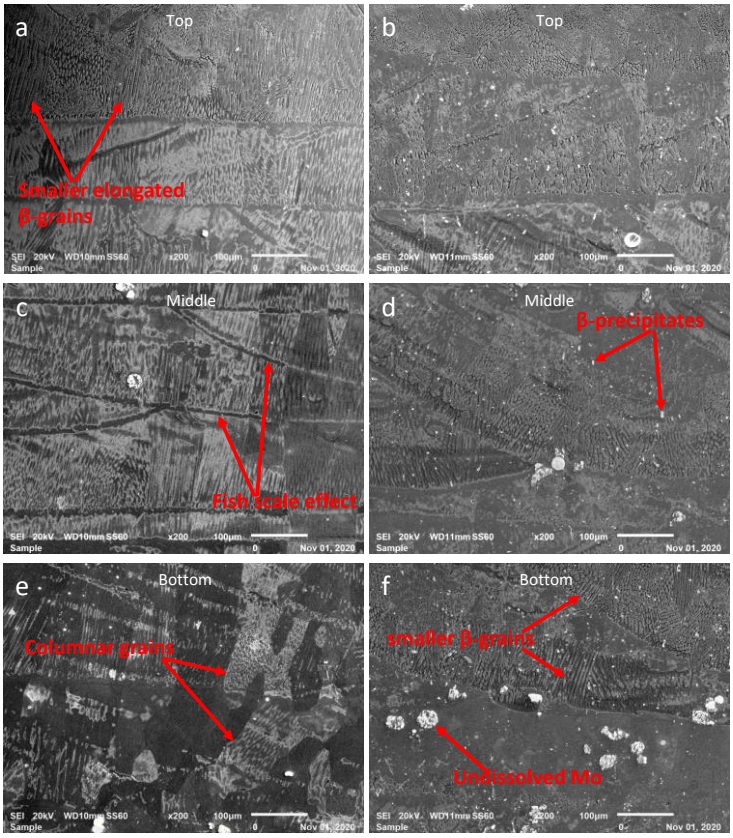

Figure 5: SEM imaging of pre-mixed (a, c, e) and LENS blend alloys (b, d, f) Ti6Al4V ELI+20%Mo produced at 287 J/mm^3

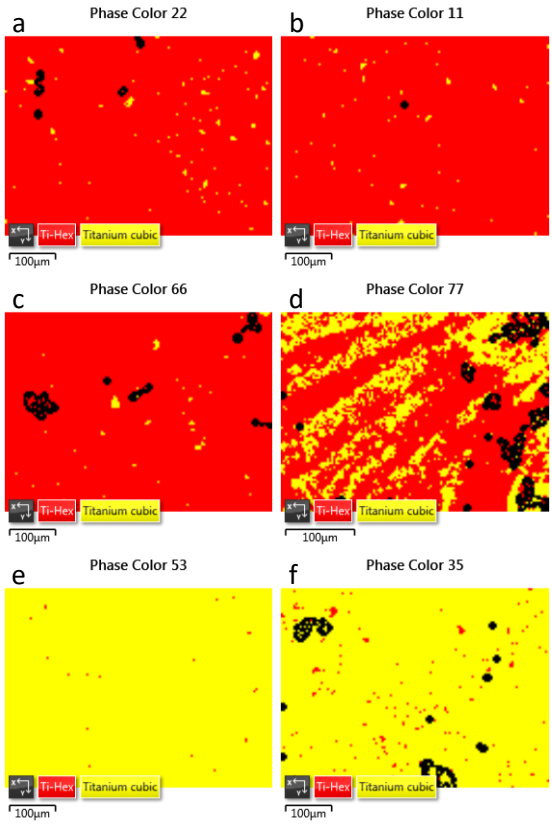

Figure 6: EBSD phase maps showing influence of the Mo content on the phase composition. (a, b) Ti6Al4V ELI, (c, d) 10% Mo and (e, f) 20% Mo, pre-mixed (a, c, e) and LENS blend alloys (b, d, f)

Table 2: EBSD phase fraction analysis of as-built alloys

Alloy	**Phase**	**Fraction (%) at 235 J/mm^3**	**Fraction (%) at 287 J/mm^3**
As-built	Ti-hex (hcp)	98.01	99.13
	Ti-cubic (bcc)	1.21	0.77

Table 3: EBSD phase fraction analysis of pre-mixed and LENS blend alloys at 287 J/mm^3

Alloy	Phase	Pre-mixed Fraction, %	LENS Blend Fraction, %
10% Mo	Ti-hex (hcp)	96.87	64.07
	Ti-cubic (bcc)	0.81	29.4
20% Mo	Ti-hex (hcp)	0.17	1.59
	Ti-cubic (bcc)	99.83	95.55

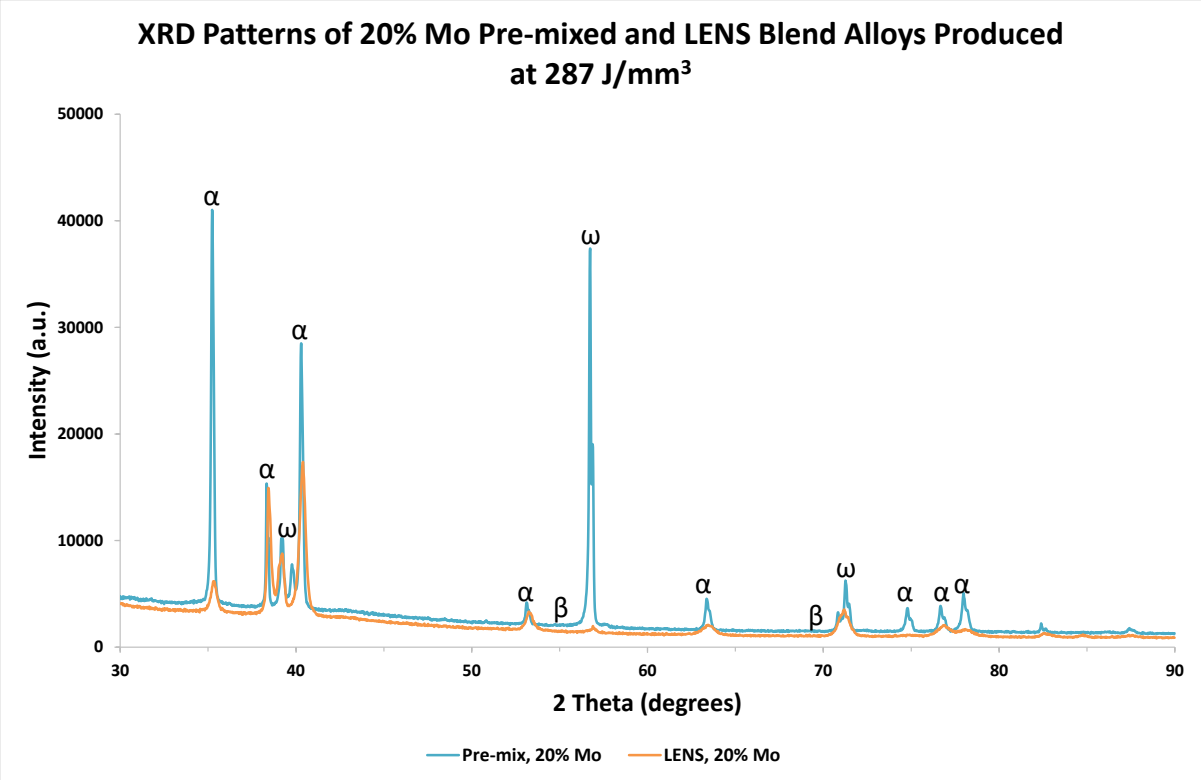

Figure 7: XRD patterns of 20% Mo Pre-mixed and LENS blend alloys produced at 287 J/mm^3

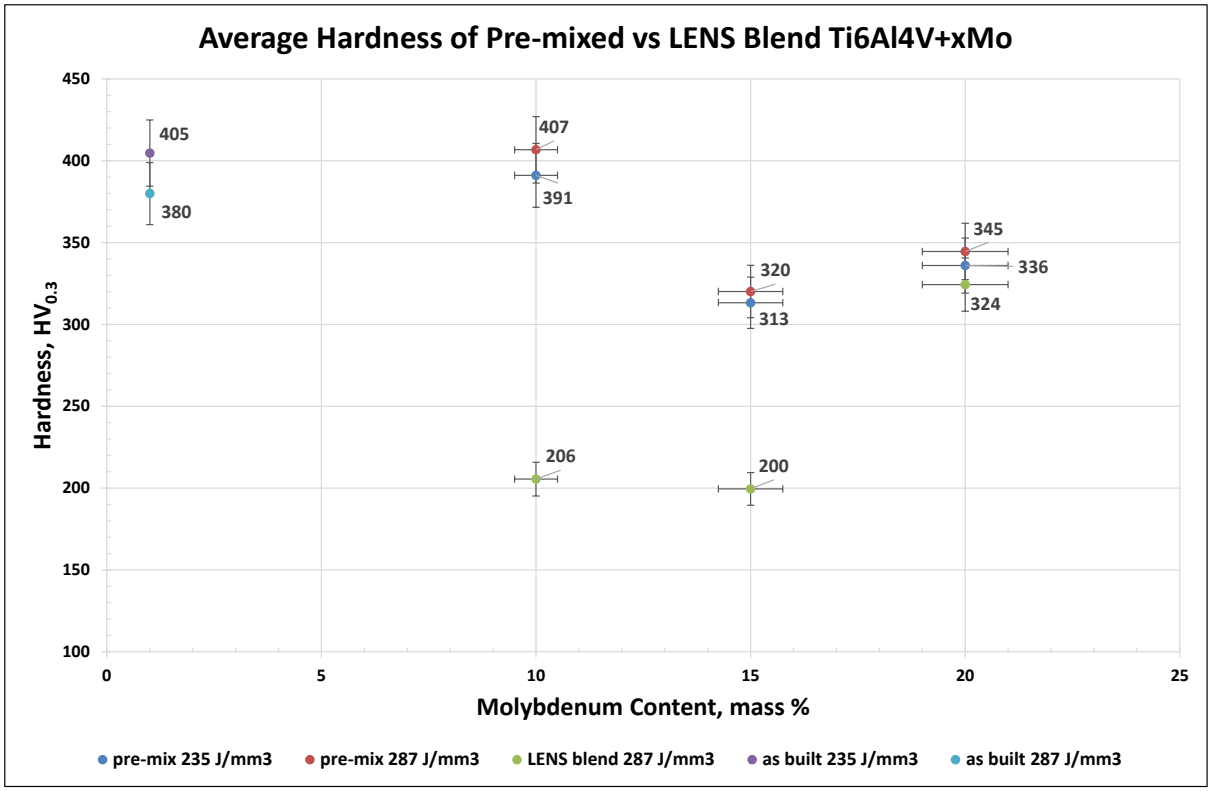

Figure 8: Average hardness as a function of Mo content of the pre-mixed and LENS blend Ti6Al4V ELI + xMo DED samples